UDC 519.6 **DOI: 10.20998/2222-0631.2025.02(9).16**

***L. SCHEK, E. N. VILCHEVSKAYA, W. H. MÜLLER***

# COMPUTATIONAL ANALYSIS OF THE DEFORMATION BEHAVIOR OF 4D-PRINTED LIQUID CRYSTAL ELASTOMERS UNDER CHANGE OF TEMPERATURE

This paper focuses on an FE simulation of Liquid Crystal Elastomers (LCE). For this purpose, a new method is proposed based on the combination of nonlinear deformation analysis based on a St. Venant – Kirchhoff law, i.e., a physically linear but geometrically nonlinear stress-strain relationship. The deformation gradient is decomposed multiplicatively into elastic, (classical) thermal, and phase transformation parts. For the transformation part a novel representation is chosen based on an orientation parameter within a distribution function for the mesogens. This parameter can be linked to temperature. The stiffness tensor in the St. Venant – Kirchhoff law as well as the tensor of thermal expansion (for the thermal part of the deformation gradient) are obtained from Mori-Tanaka homogenization schemes. It is shown that classical thermal expansion with positive expansion coefficients and realistic values does not contribute much to the total large deformations. The mayor contribution comes from phase transformation. It is, therefore, misleading to model the deformation of LCEs during temperature change by classical thermal expansion, although exactly this is done in the literature by a trick–namely, using negative anisotropic thermal expansion coefficients.

**Key words:** 4D printing, liquid crystal elastomer, FE simulation, Mori-Tanaka scheme, distribution function, shape function.

***Л. ШЕК, Е. Н. ВІЛЬЧЕВСЬКА, В. Г. МЮЛЛЕР***

# ОБЧИСЛЮВАЛЬНИЙ АНАЛІЗ ДЕФОРМАЦІЙНОЇ ПОВЕДІНКИ РІДКОКРИСТАЛІЧНИХ ЕЛАСТОМЕРІВ, НАДРУКОВАНИХ ЗА ДОПОМОГОЮ 4D-ДРУКУ, ПРИ ЗМІНІ ТЕМПЕРАТУРИ

Ця стаття зосереджена на моделюванні методом скінченних елементів рідкокристалічних еластомерів (РКЕ). Для цього запропоновано новий метод, заснований на комбінації нелінійного аналізу деформації на основі закону Сен-Венана – Кірхгофа, тобто фізично лінійної, але геометрично нелінійної залежності напруження-деформації. Градієнт деформації мультиплікативно розкладається на пружну, теплову та фазово-перетворювальну частини. Для перетворювальної частини вибрано нове представлення на основі параметра орієнтації в межах функції розподілу мезогенів. Цей параметр може бути пов'язаний з температурою. Тензор жорсткості в законі Сен-Венана – Кірхгофа, а також тензор теплового розширення (для теплової частини градієнта деформації) отримані зі схем гомогенізації Морі-Танаки. Показано, що класичне теплове розширення з позитивними коефіцієнтами розширення та реалістичними значеннями не робить значного внеску в загальну величину великих деформацій. Тому моделювання деформації РКЕ під час зміни температури за допомогою класичного теплового розширення є помилкою, хоча саме це робиться в літературі за допомогою хитрощів, а саме, використовуючи негативні анізотропні коефіцієнти теплового розширення.

**Ключові слова:** 4D-друк, рідкокристалічний еластомер, моделювання методом скінченних елементів, схема Морі-Танаки, функція розподілу, функція форми.

**Introduction.** 4D printing of *liquid crystal elastomers (LCEs)* is an emerging field that combines the anisotropic responsiveness of LCEs with additive manufacturing techniques to create structures capable of dynamic, stimuli-induced shape transformations over time [1]. LCEs are crosslinked polymer networks that incorporate liquid crystalline *mesogens*. These mesogens can be aligned during fabrication, enabling the material to undergo reversible, anisotropic deformations in response to external stimuli such as heat (temperature change), light, or electric fields. This unique combination of properties makes LCEs particularly suitable for 4D printing applications, where time-dependent shape changes are desired [2]. Several additive *manufacturing methods* have been adapted for 4D printing of LCEs:

- *Direct Ink Writing (DIW)* [3]: This extrusion-based technique allows for the alignment of mesogens along the printing path due to shear forces during extrusion. Post-printing, the structures are typically cured using UV light to fix the alignment. DIW is noted for its flexibility and rapid printing speed [3].
- *Vat Photopolymerization* (e.g., SLA and DLP) [3]: These methods use light to cure photosensitive resins layer by layer, achieving high-resolution prints. They are particularly useful for creating complex geometries with fine features.
- *Inkjet Printing*: This technique deposits tiny droplets of material to build up structures and is valued for its high resolution and ability to handle multiple materials simultaneously.

Each method offers distinct advantages and is chosen based on the desired properties and applications of the final LCE structure [4]. LCEs exhibit several key properties that make them ideal for 4D printing:

- *Stimuli-Responsive Behavior* [4]: They can undergo significant, reversible shape changes when exposed to external stimuli.
- *Programmable Anisotropy* [2], [5]: The directionality of deformation can be programmed during fabrication by controlling the alignment of mesogens.
- *Complex Deformation Modes* [2]: By designing specific mesogen alignments, LCEs can achieve intricate movements such as bending, twisting, and folding.

The unique properties of 4D-printed LCEs open up a range of applications:

- *Soft Robotics* [1]: Creating actuators and robotic components that can move and adapt their shape in response to stimuli.
- *Biomedical Devices* [5]: Developing implants or drug delivery systems that change shape or function within the body.

- *Optical Devices* [6], [7]: Fabricating components that alter their optical properties through shape changes.

*Wearable Technology:* Designing garments or accessories that adapt to environmental conditions or user needs.

**Simulating the deformation of LCEs.** The deformation behavior of LCEs has been extensively studied using various simulation methodologies, each capturing different aspects of their complex, stimuli-responsive mechanics. These approaches range from continuum mechanics models to molecular simulations, providing insights at both macroscopic and microscopic scales. Below is a summary of the primary simulation methods employed so far:

*Continuum Mechanics Models*

- *Neoclassical Theory*: This framework extends classical rubber elasticity to LCEs by incorporating the anisotropic nature of liquid crystal mesogens. It models the coupling between mechanical deformation and mesogen orientation, effectively capturing soft elasticity and large deformations [8].
- *Pseudo-Anelastic Models*: To account for stress softening and residual strains observed in LCEs under cyclic loading, pseudo-anelastic models introduce separate strain-energy functions for loading and unloading phases. This approach allows for the simulation of Mullins-like effects within LCEs [9].
- *Ogden-Type Strain-Energy Functions*: These phenomenological models are adept at representing complex elastic behaviors, including the auxetic response (negative Poisson's ratio) observed in certain LCEs under large strains [10].

*Finite Element Analysis (FEA)*

- *Thermomechanical Simulations*: FEA has been utilized to simulate the bending and curling behaviors of LCE beams under thermal stimuli. By incorporating temperature-dependent strain differences due to mesogen alignment, these models predict deformation patterns such as bending angles and curvature [11].
- *Mechanical Instabilities and Pattern Formation*: Advanced FEA models have been developed to study phenomena like wrinkling and buckling in LCEs. These simulations consider factors like material heterogeneity and external constraints to predict complex deformation modes [12].

*Molecular Simulations*

- *Monte Carlo (MC) Simulations*: MC methods have been employed to investigate the molecular-level behavior of LCEs, particularly focusing on the effects of electric fields and temperature changes on mesogen orientation and network deformation. These simulations provide insights into the microscopic mechanisms driving macroscopic actuation [13].
- *Molecular Dynamics (MD) Simulations*: Coarse-grained MD simulations have been used to study the relationship between molecular architecture and mechanical properties in LCEs. These models help in understanding how variations in crosslink density and mesogen alignment affect the overall material behavior [14].

*Phase Field Modeling*

- *Domain Evolution and Polydomain Structures*: Phase field models couple the elastomer network's mechanical energy with the liquid crystal's free energy to simulate the evolution of domain structures within LCEs. This approach is particularly useful for studying the formation and dynamics of polydomain configurations under various stimuli [15].

*Geometric and Reduced-Order Models*

*Bending-Twisting Rod Models*: Reduced-order models, such as those based on the Kirchhoff rod theory, have been adapted to LCEs to simulate bending and twisting behaviors. These models incorporate the coupling between curvature, torsion, and mesogen orientation to predict complex deformations in slender LCE structures [16].

**Mathematical Model.** We consider LCEs as a heterogeneous material consisting of an isotropic matrix with stiffness $C_0$ and thermal expansion coefficient $\alpha_0$, containing a large number of uniformly distributed mesogens, which we idealize as spheroids with equatorial axes $a$ and polar axis $a_3$, composed of an isotropic material with properties $C_1$ and $\alpha_1$. The mesogens exhibit a certain degree of orientation after the printing and curing process at low temperatures. However, as the temperature increases, they are able to rotate freely, leading to a random orientation distribution when the temperature reaches $T_{iso}$, as illustrated in the top row of Fig. 1. At this stage, we neglect internal stresses that may arise due to mesogen rotation. Moreover, we do not consider the internal dynamics of the process, and instead study a sequence of quasi-static thermomechanical states of the heterogeneous material under varying degrees of mesogen alignment.

In continuum mechanics, the primary elements are material particles whose macroscopic thermomechanical properties are understood as effective quantities obtained by averaging the corresponding meso-scale fields. Unlike classical approaches, we assume that a change in the degree of alignment of micro-particles not only alters the effective elastic moduli and thermal expansion coefficient, but also results in a change in the effective shape of the macro-particle. Fig. 1 illustrates the underlying transition process from the molecular to the continuum level: three different situations of *the Representative Volume Element (RVE)* of the LCE are shown. Shown on the left is the ideal low-temperature scenario, where all mesogens are perfectly aligned. On the continuum level this corresponds to a very slender spheroid. In the RVE on the right the high temperature situation is shown, where the mesogens are isotropically (better: fully randomly) oriented. On the continuum level this corresponds to a sphere. Finally, at some intermediate temperature $T(t)$ at time $t$ we find less order but not complete chaos, which corresponds to a spheroid on its way to become a sphere. Traditionally, such effects are modeled using a micromorphic continuum, which significantly complicates the model. Theories have been proposed on that subject, *notably by Eringen* [17]. However, in this article we do not make any use of them. We propose instead to treat the degree of particle alignment as an additional degree of freedom, the variation of which induces transformation deformations $F^{\text{tr}}$ at the macroscopic level.

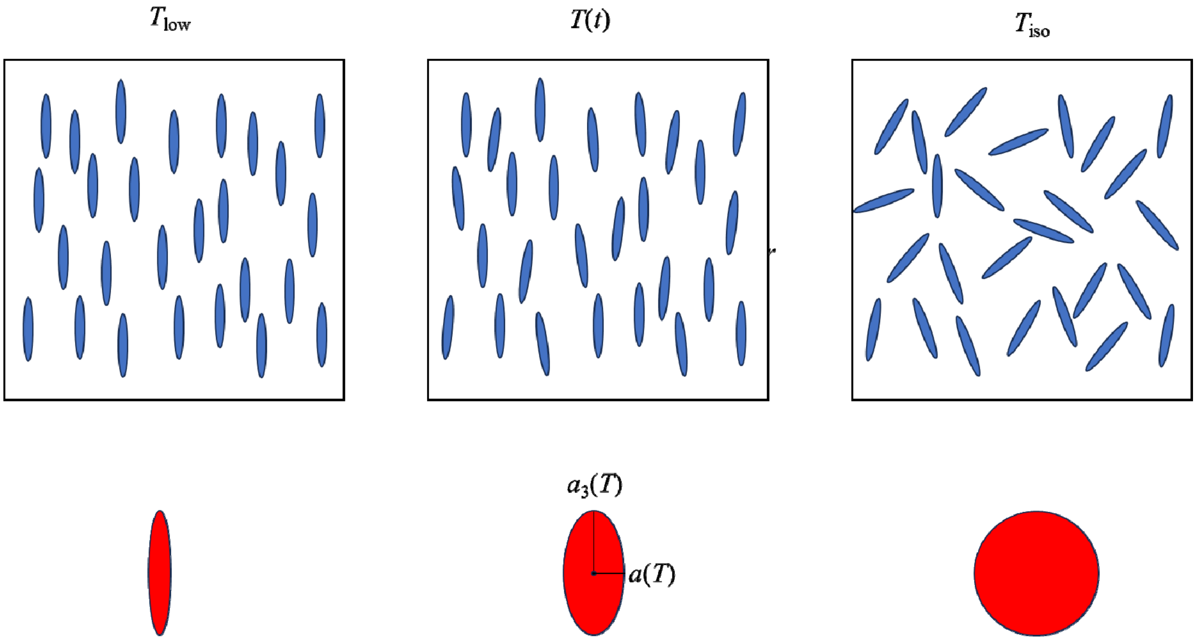

Fig. 1 – Illustrating the transition from the molecular (first row) to the continuum level (second row).

Thus, within this approach, the primary macroscopic quantities are characterized by the degree of alignment of the mesogens relative to a prescribed direction $m$. Let us denote by $n$ the symmetry axis of an individual spheroid, with its deviation from the given direction $m$ described by the angle $\varphi$. The randomness of the direction of the deviation implies transverse isotropy of the overall properties and allows us to introduce a probability density function of the form [18], Section 5.3.5:

$$\psi_\lambda(\varphi) = \frac{1}{2\pi}\left[\left(\lambda^2+1\right)e^{-\lambda\varphi} + \lambda e^{(-\lambda\pi/2)}\right], \text{ with } \int_\Phi \psi_\lambda(\varphi)\,d\Phi = 1, \tag{1}$$

where $d\Phi$ refers to integration over half of the unit sphere, and the scatter parameter $\lambda$ characterizes the degree of anisotropy.

The behavior of $\psi_\lambda(\varphi)$ for different values of $\lambda$ is shown in Fig. 2: the smaller $\lambda$, the closer we get to an isotropic distribution of mesogens and for $\lambda \to \infty$ we get a perfect orientation in $m$ – direction, i.e., to the transversally isotropic state. We can link this parameter to the temperature $T$ whilst we know that at high temperatures $T_{iso}$ the isotropic state prevails. This is achieved by means of the following empirical assignment:

$$\lambda = \lambda(T) = \frac{\lambda_\infty}{2}\left(1 - \tanh\frac{\dfrac{T}{T_{iso}} - \alpha}{\beta}\right). \tag{2}$$

In here $\lambda_\infty$ is a sufficiently large number, which characterizes the relatively ordered state of the mesogens right after printing (typically at room temperature). Moreover, $\alpha$ and $\beta$ are two parameters for scaling and shifting, see Fig. 3.

To obtain $F^{\text{tr}}$ we first note the shape tensor of an individual spheroid in the form:

$$A = a\left(1 - nn\right) + a_3 nn, \tag{3}$$

where $1$ is the unit tensor and $n$ is a unit vector in direction of the polar axis, and $1 - nn$ is a projection operator onto the plane of isotropy. In spherical coordinates we have:

$$n=\cos\theta\sin\varphi e_1+\sin\theta\sin\varphi e_2+\cos\varphi e_3\,. \tag{4}$$

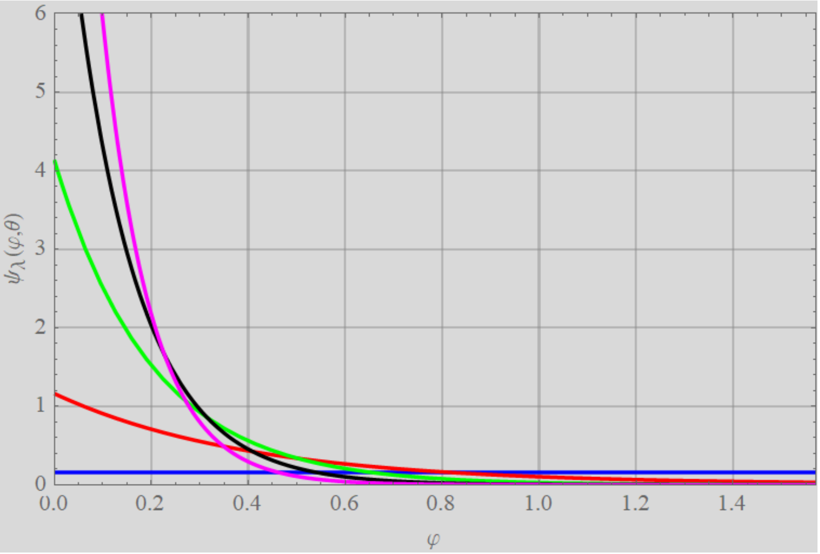

Fig. 2 – Distribution function $\psi_\lambda(\varphi)$ for different values of $\lambda=0$ (blue), $2.5$ (red), $5$ (green), $7.5$ (black), $10$ (magenta).

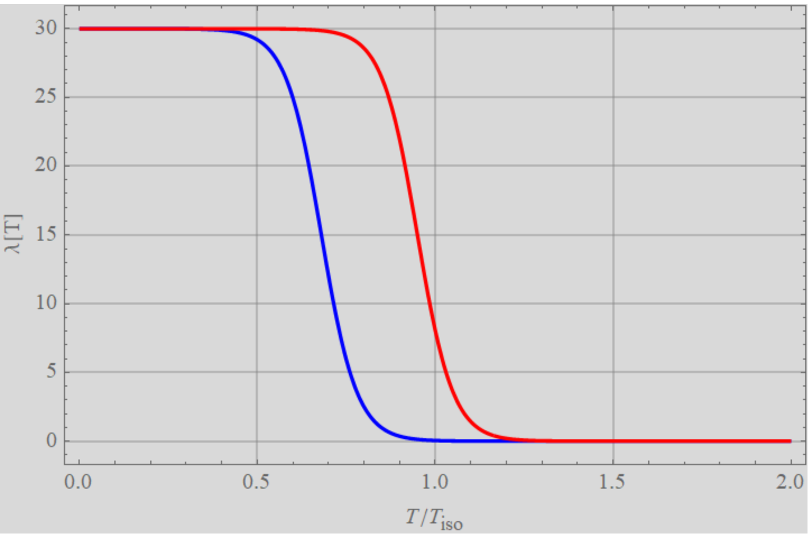

Fig. 3 – Orientation parameter as a function of temperature, $\lambda(T)$, for $\lambda_\infty=30$ and $\alpha=0.68$ (blue), $\alpha=0.95$ (red), $\beta=0.1$.

Consequently, the average shape tensor for the spheroid on the continuum scale can be obtained by means of the distribution function from Eq. (1) through homogenization by integration over (half) the unit sphere $\Phi$:

$$\langle A\rangle=\int_\Phi A\psi_\lambda(\varphi)\,d\Phi \tag{5}$$

and we obtain

$$\langle A\rangle=a(\lambda)(1-mm)+a_3(\lambda)mm \tag{6}$$

with

$$a(\lambda)=a\left[1+(\gamma-1)\frac{18-\exp(-\lambda\pi/2)\lambda\left(8+\lambda^2\right)}{6\left(9+\lambda^2\right)}\right],\quad a_3(\lambda)=a_3\left[\frac{1}{\gamma}+\left(1-\frac{1}{\gamma}\right)\frac{\left[3+\exp(-\lambda\pi/2)\lambda\right]\left(3+\lambda^2\right)}{3\left(9+\lambda^2\right)}\right]. \tag{7}$$

In here $\gamma=a_3/a$ is known as *the aspect ratio*. In the present case of the LCE mesogens we have typically $\gamma\approx 5$ [19]. This means our spheroid is of prolate shape.

Introducing the transformation deformations as a tensor that links the initial and current shape, $\langle A\rangle=F^{\text{tr}}\cdot\langle A\rangle(\lambda_\infty)$, we find that

$$F^{\mathrm{tr}}=\frac{a(\lambda)}{a(\lambda_\infty)}(1-mm)+\frac{a_3(\lambda)}{a_3(\lambda_\infty)}mm\,. \tag{8}$$

**Geometrically nonlinear stress strain relation.** We use a multiplicative decomposition of the deformation gradient,

$$F=F^{el}\cdot F^{\mathrm{th}}\cdot F^{\mathrm{tr}}\,, \tag{9}$$

with, $F^{\mathrm{th}}$ and $F^{\mathrm{el}}$ being the contributions related to classical thermal, and (nonlinear) elastic respectively.

Now recall the definition of *the Green-Lagrange strain tensor*, applied only to the elastic deformation:

$$E^{\mathrm{el}}=\frac{1}{2}\left(C^{el}-1\right),\ C^{el}=\left(F^{el}\right)^T\cdot F^{el}. \tag{10}$$

This strain tensor is used in *the St. Venant–Kirchhoff constitutive law* [20]:

$$S=C_{\mathrm{hom}}(\lambda):E^{el},\ S=\det F^{el}\left(F^{el}\right)^{-1}\cdot\sigma\cdot\left(F^{el}\right)^{-T}, \tag{11}$$

where $S$ is *the second Piola-Kirchhoff stress*, $\sigma$ is *the Cauchy stress tensor*, and $C_{\mathrm{hom}}(\lambda)$ is the fourth order homogenized stiffness tensor, derived from the properties of the matrix and the mesogens using ***the Mori–Tanaka scheme***. Since homogenization via the Mori-Tanaka approach is a well-established method–particularly effective even for higher volume fractions of inclusions–we present here only the final expression:

$$C_{\mathrm{hom}}(\lambda)=C_0+p\left(p\left(C_1-C_0\right)^{-1}+(1-p)\left\langle{}^4\overline{N}\right\rangle^{-1}\right)^{-1}, \tag{12}$$

where $p$ is the volume fraction of mesogens, and the (averaged) stiffness contribution tensor,

$$\left\langle{}^4\overline{N}\right\rangle=\int_\Phi{}^4\overline{N}\psi_\lambda(\varphi)d\Phi,\ {}^4\overline{N}=\left[\left(C_1-C_0\right)^{-1}+{}^4P\right]^{-1}, \tag{13}$$

which is a function of $\lambda$. Moreover, ${}^4P$ denotes *Hill's tensor*, which characterizes the strain at a point $x$:

$${}^4P=\left(\nabla\int_{V_{\mathrm{in}}}G(x-x')\nabla'dx'\right)^s_{(12)(34)}, \tag{14}$$

where $V_{\mathrm{in}}$ is the volume of an inclusion, $G(x-x')$ is *the Green's function for displacement*, and $s$ indicates appropriate symmetrization. For an ellipsoidal domain ${}^4P$ is a constant and depends on the shape of the inclusion. Specific values of ${}^4P$ and further information on Eq. (12) are provided in **Appendix B**.

For the thermal part of the deformation gradient, we assume the following form:

$$F^{\mathrm{th}}=\left(1+\alpha_{\mathrm{hom},1}(\lambda)\Delta T\right)(1-mm)+\left(1+\alpha_{\mathrm{hom},3}(\lambda)\Delta T\right)mm\,, \tag{15}$$

where the homogenized coefficients of thermal expansion, $\alpha_{\mathrm{hom},1/3}(\lambda)$, can also be computed via homogenization. A detailed derivation under *the Mori–Tanaka framework* is provided in **Appendix C**:

$$\alpha_{\mathrm{hom}}(\lambda)=\alpha_0+p\left\{\left[p\,{}^41+(1-p)\left\langle{}^4\overline{H}_T\right\rangle^{-1}\right]^{-1}:\left({}^41-\left\langle{}^4\overline{H}_T\right\rangle^{1}\right)+\left\langle{}^4\overline{H}_T\right\rangle^{-1}\right\}:\left(\alpha_1-\alpha_0\right)\Delta T\,. \tag{16}$$

Here $\alpha_0$ and $\alpha_1$ are isotropic thermal expansion tensors known from experimental data, $\Delta T$ is the temperature change, and ${}^41$ is the fourth-order identity tensor. The extended (averaged) compliance contribution tensor $\left\langle{}^4\overline{H}_T\right\rangle$ is defined as:

$$\left\langle{}^4\overline{H}_T\right\rangle=\int_\Phi{}^4\overline{H}_T\psi_\lambda(\varphi)d\Phi,\ {}^4\overline{H}_T=\left[{}^41+\left(S_1-S_0\right):{}^4Q\right]^{-1}, \tag{17}$$

where $S_k=C_k^{-1}$ are the compliance tensors of the matrix and the inclusions, and ${}^4Q=C_0-C_0:{}^4P:C_0$. $\left\langle{}^4\overline{H}_T\right\rangle$ is also a function of $\lambda$.

**Homogenization schemes applied to LCEs.** We assign to the elastomer matrix $\mu_0\approx1\,\mathrm{MPa}$ and $k_0=\lambda_0+$ $+\frac{2}{3}\mu_0\approx10\,\mathrm{MPa}$ (see [21] for typical values). The mesogens are essentially rigid (see [22]). Fig. 4 shows results for the homogenized stiffnesses $C_{\text{hom}}(\lambda)$ for $\mu_1 = 10\mu_0$, $k_1 = 10k_0$ (computed by using (12)) on the left and for rigid inclusions (computed with (50)) on the right, both for a volume fraction $p = 0.3$ (chosen for demonstration purposes). Recall that high values of $\lambda$ correspond to the transversally isotropic state at room temperature and $\lambda = 0$ to the isotropic state at higher temperatures (ca. $100^\circ\text{C}$). The difference between the two plots at high temperatures ($\lambda = 0$) is small. As expected, the stiffnesses in the direction of transversal axis are higher at room temperature (large $\lambda$) in the rigid case. For higher volume fractions $p$ the values increase accordingly.

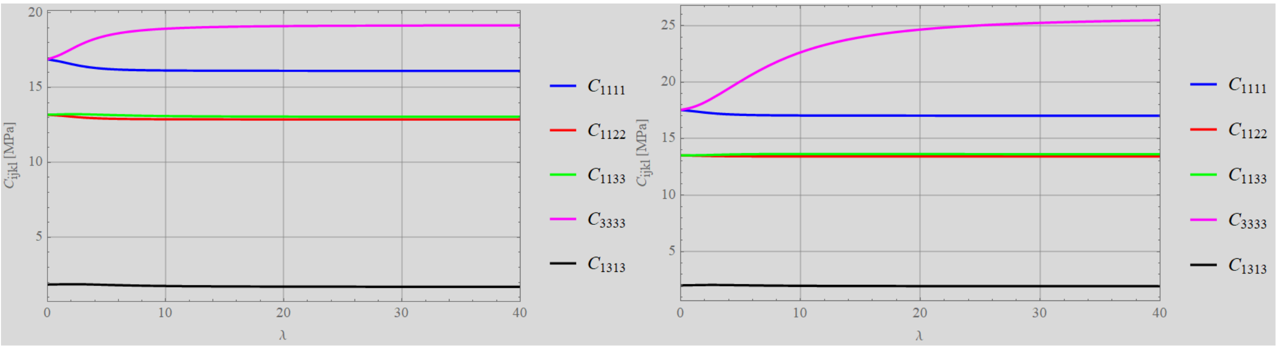

Fig. 4 – Homogenized stiffnesses $C_{\text{hom}}(\lambda)$, see text.

For the (isotropic) thermal expansion of the matrix we choose $\alpha_0 = 80\,\text{ppm}/\text{K}$ (elastomer matrix) and for the mesogens $\alpha_1 = 40\,\text{ppm}/\text{K}$ (see [23]). From (16) we obtain the result shown in Fig. 5 for a volume fraction $p = 0.3$ using the stiffnesses from before. The blue curve stands for the coefficients within the isotropic plane $\alpha_{\text{hom},1} = \alpha_{\text{hom},2}$ and the red one for the transverse direction $\alpha_{\text{hom},3}$.

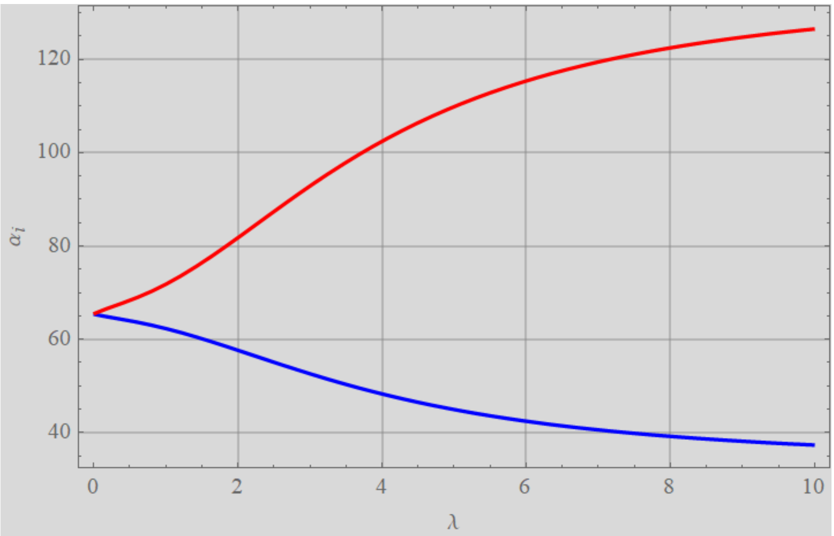

Fig. 5 – Homogenized thermal expansion tensor $\alpha_{\text{hom}}(\lambda)$ in ppm/K, see text.

**Simulation of nonlinear deformations.** As a first example we shall now model the deformation of double layer LCE sheets as described in [24] within the framework of our method. Such LCE sheet structures are also mentioned in [25], Fig. 12 and [26]. They are simple and serve perfectly to illustrate the point without distracting the attention of the reader by complicated geometries. Clearly, for technical applications, more complicated shapes should be studied.

As shown in Fig. 6 a double, perpendicularly printed rectangular LCE structure is heated up from room temperature to about $100^\circ\text{C}$. As noted in the supporting information to [24] the sheets are typically $35 \times 5\,\text{mm}$ in dimension. The sample thickness varies between ca. $0.5$ and $2\,\text{mm}$. In the real experiment the heating is achieved by electric currents through internal wiring as indicated in the cartoon. The clamping visible in the second row of pictures is definitely not the one used in technical mechanics when studying statically determinate systems. It is probably somewhat close to a rigid support. A strongly non-linear smiley-type deformation behavior is observed that leads to curling of the specimen. It is therefore not surprising that one technical application of LCEs is to use them as grippers [27], [28], [29], Fig. 77.

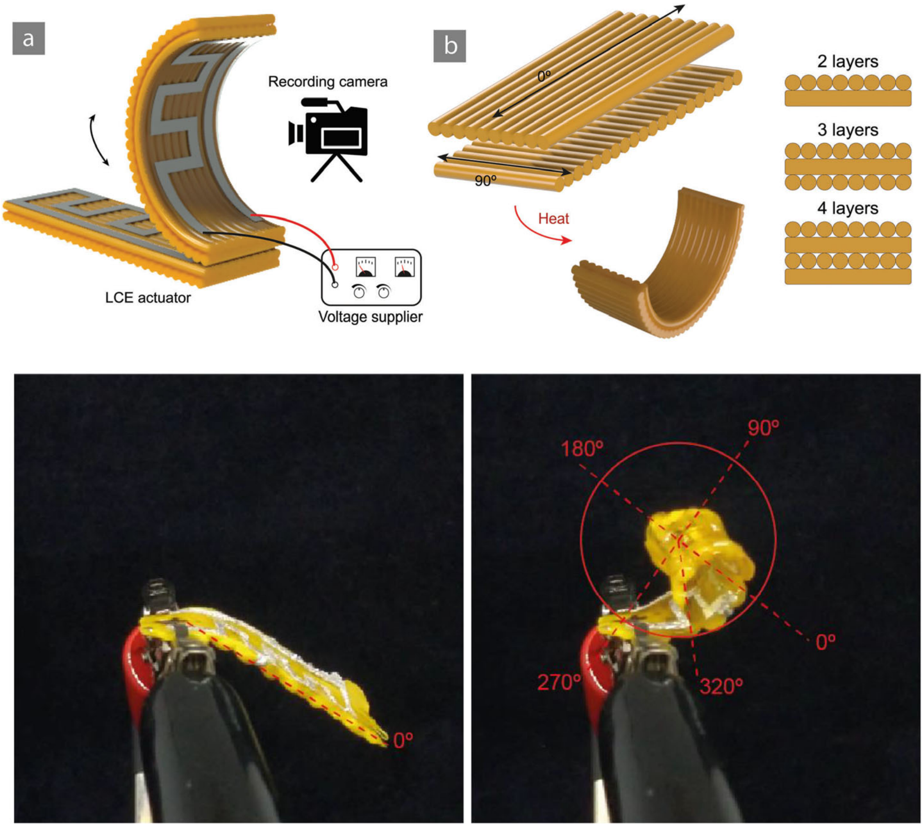

Fig. 6 – LCE double layer sheet structures and their highly non-linear deformation behavior during temperature change starting from room temperature (flat) to about $100^\circ\mathrm{C}$, top: cartoon, bottom: reality (all figures from [24]).

In our simulations, Eqs. (9) – (17) are solved numerically using the programmable finite element software FEniCS [30]. The mesh including dimensions is shown in Fig. 7. A $40\times 8\times 12$ hexagonal mesh, which is subdivided into tetrahedra was used. The trial functions were linear in order to reduce computation time. The top half of the FE-model shows a printing direction $m = e_1$ and the bottom half has been assigned $m = e_3$. Also, the side plane was constrained with one node completely fixed, and all others only fixed in $x$–direction, allowing for free sliding in the two other directions, so that no artificial stresses would occur at the supported end. The resulting deformation pattern shown in Fig. 8 has a remarkable resemblance to the cartoon as well as to the experimental result shown in Fig. 6. It should be stressed again that this simulation is based on realistic data and by using the concept of the temperature dependent orientation parameter $\lambda$ alone. No tricks are involved.

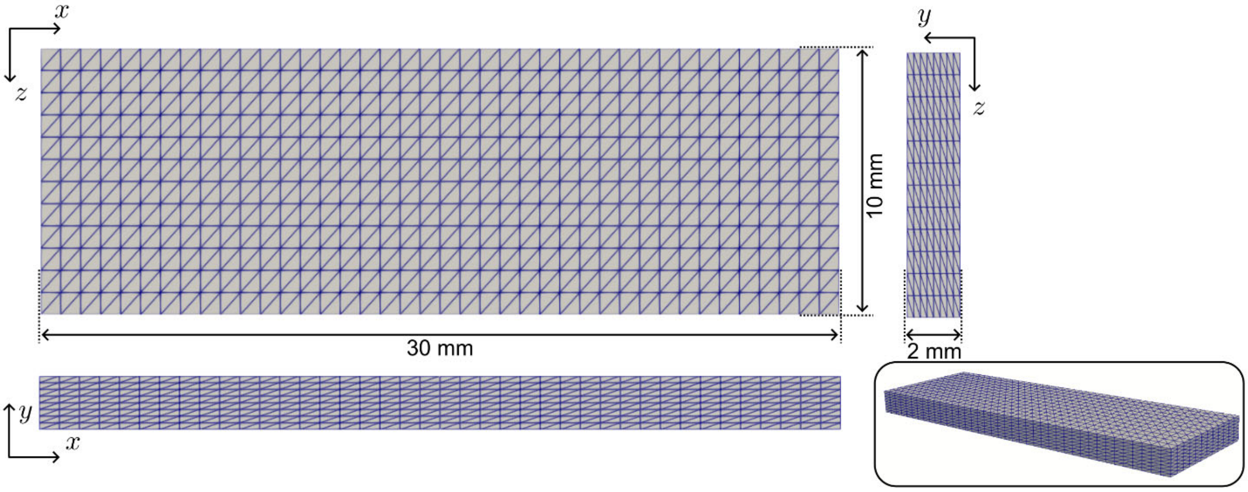

Fig. 7 – FE-mesh used during simulations.

Next, we explore the effect of classical thermal expansion on deformation alone. In order to get a visible effect, we use *constant* extreme values from Fig. 5, namely in printing direction $m$ we choose $\approx 120\,\text{ppm/K}$ and in the perpendicular directions $\approx 40\,\text{ppm/K}$. But even then, the effect shown in Fig. 9 is small compared to the deformation from phase transition in Fig. 8. In hindsight one should say that the computation of $\alpha_{\text{hom}}(\lambda)$ based on the Mori-Tanaka scheme was perfectly legitimate, because its application is limited to small deformations.

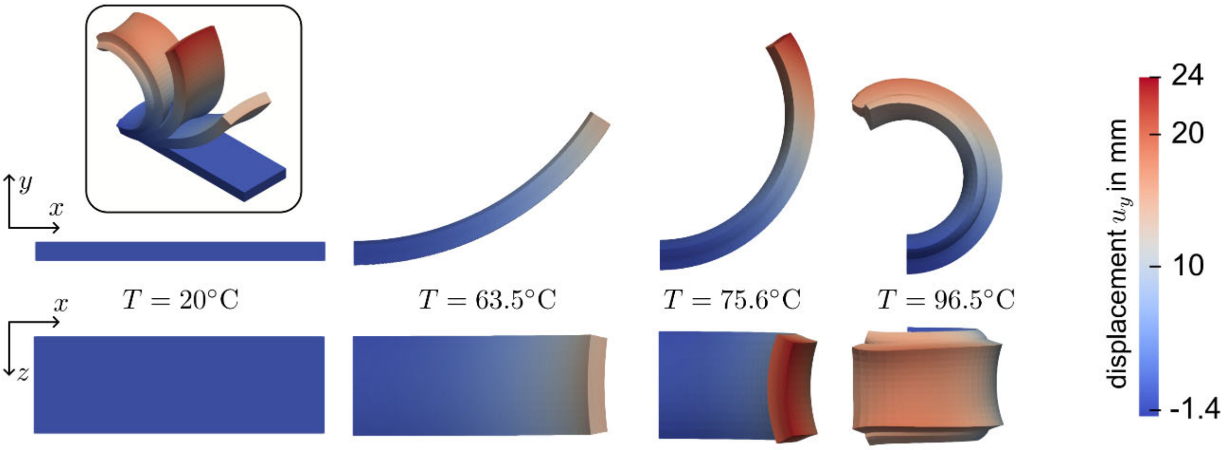

Fig. 8 – Orientation parameter $\lambda$ based modeling of a LCE double layer sheet structure and its highly non-linear deformation behavior during temperature change starting from room temperature (flat) to about $100^{\circ}\text{C}$.

We now follow a suggestion for modeling the deformation behavior suggested in [31]: "LCE was modeled as a linear thermoelastic material with anisotropic thermal expansion coefficients and a Poisson's ratio of 0.499. The thermal expansion coefficient $\alpha$ was determined from the measurements presented in [left out intentionally], and the thermal expansion coefficients in the directions perpendicular to the axial direction were set as $-\alpha/2$". The use of anisotropic expansion coefficients with negative values is clearly a dirty trick to model the large deformations, albeit an effective one. We extended it somewhat and put

$$F^{\text{th}} = (1-\alpha\,\Delta T)e_1e_1 + \frac{1}{\sqrt{1-\alpha\,\Delta T}}(e_2e_2 + e_3e_3)\,. \tag{18}$$

The use of a square root goes back to [32]. With the fictive value $\alpha = 3500\,\text{ppm}/\text{K}$, we obtain the result shown in Fig. 10. It is very similar to Fig. 8, indeed, but it is based on questionable premises, and, what is more, the value chose for the coefficient of thermal expansion is absurdly large.

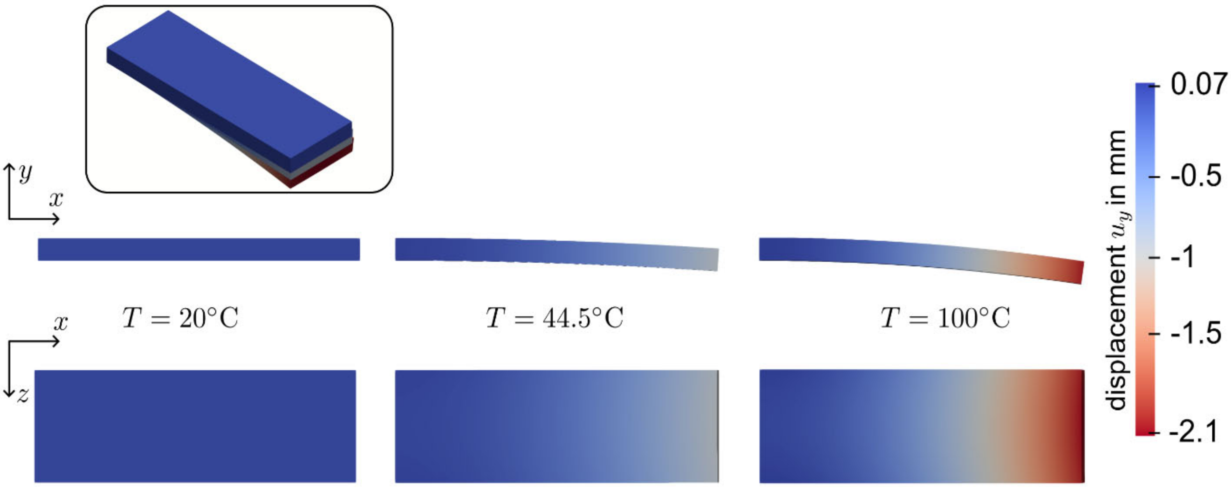

Fig. 9 – LCE double layer sheet structures modeled by assuming regular thermal expansion only.

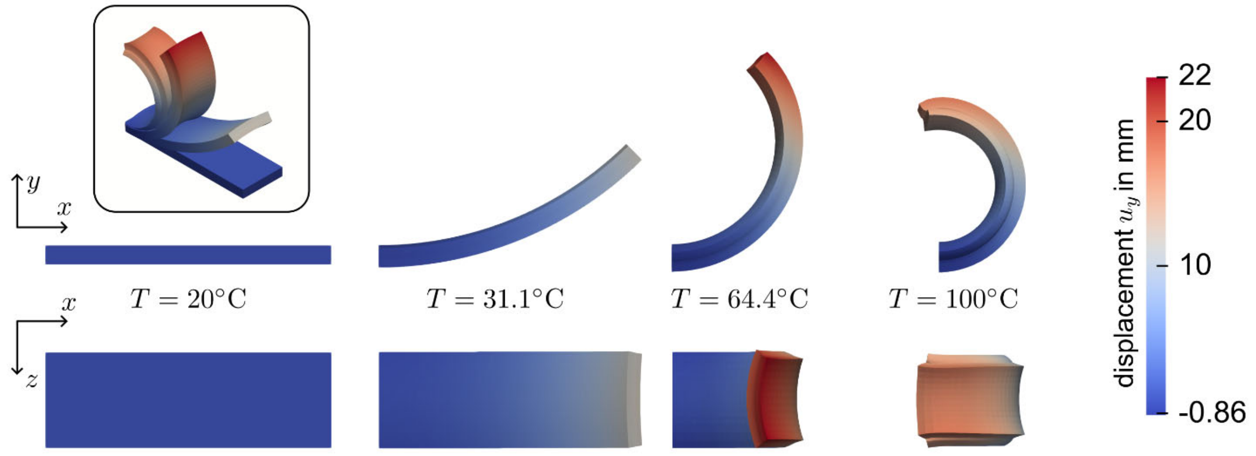

Fig. 10 – LCE double layer sheet structures modeled by assuming (artificial) negative anisotropic thermal expansion coefficients.

**Conclusions.** Thus, in this work, we presented, first, an overview on the making (4D-printing) and currently used simulation techniques applied in context with Liquid Crystal Elastomers (LCEs). Second, the thermo-mechanical setting was presented: nonlinear deformation together with the new concept of a temperature-dependent orientational parameter, characterizing the distribution of the LCE mesogens, to be used in a St. Venant – Kirchhoff stress-strain relationship. Third, the basics of homogenization techniques required for effective stiffnesses and thermal expansion coefficients as a function of the orientational parameter were presented. The use of this parameter was critically examined in context with higher continuum theories. In order to be capable of accounting for high volume concentrations of mesogens Mori-Tanaka schemes were used and explained in appendices. Forth, simulations based on the new concept were presented and compared to the commonly used modeling way with anisotropic negative thermal expansion coefficients. It was shown that the latter had to be unreasonably large to create adequate results, which is not necessary when using the newly proposed method of an orientational parameter.

**Appendix (a): Some information about transversally isotropic tensors of the fourth rank.** For transversely-isotropic tensors ${}^4A$ it is convenient to use a tensor base consisting of the following six tensors ${}^4T_i$:

$$ {}^4A = \sum\nolimits_{i=1}^{6} a_i \, {}^4T_i \qquad (19)$$

with

$$ {}^4T_1 = \overline{11},\ \ {}^4T_2 = {}^41 - \frac{1}{2}\overline{11},\ \ {}^4T_3 = \bar{1}mm,\ \ {}^4T_4 = mm\bar{1}, $$

$$ {}^4T_5 = \frac{1}{4}\left(e_k m e_k m + m e_k m e_k + m e_k e_k m + e_k m m e_k\right),\ \ {}^4T_6 = mmmm, $$

$$ \bar{1} = 1 - mm,\ \ {}^41 = \frac{1}{2}\left(e_k e_s e_k e_s + e_k e_s e_s e_k\right),\ \ e_k, e_s \perp m, k, s \in 1, 2. \qquad (20)$$

The multiplication table for the $T$-tensors is as follows (the column represents the ${}^4B$ in a multiplication of two tensors of the fourth rank, ${}^4A : {}^4B$):

|  | ${}^4T_1$ | ${}^4T_2$ | ${}^4T_3$ | ${}^4T_4$ | ${}^4T_5$ | ${}^4T_6$ |
|---|---|---|---|---|---|---|
| ${}^4T_1$ | $2\,{}^4T_1$ | 0 | $2\,{}^4T_3$ | 0 | 0 | 0 |
| ${}^4T_2$ | 0 | ${}^4T_2$ | 0 | 0 | 0 | 0 |
| ${}^4T_3$ | 0 | 0 | 0 | ${}^4T_1$ | 0 | ${}^4T_3$ |
| ${}^4T_4$ | $2\,{}^4T_4$ | 0 | $2\,{}^4T_6$ | 0 | 0 | 0 |
| ${}^4T_5$ | 0 | 0 | 0 | 0 | ${}^4T_5/2$ | 0 |
| ${}^4T_6$ | 0 | 0 | 0 | ${}^4T_4$ | 0 | ${}^4T_6$ |

(21)

If $x_3$ is chosen as the axis of transverse symmetry, any *transversely isotropic* tensor ${}^4A$, when represented in this basis, has the following components:

$$ a_1 = \frac{A_{1111} + A_{1122}}{2},\ \ a_2 = 2A_{1212},\ \ a_3 = A_{1133},\ \ a_4 = A_{3311},\ \ a_5 = 4A_{3131},\ \ a_6 = A_{3333}. \qquad (22)$$

Moreover, the inverse Tensor ${}^4A^{-1}$ can be calculated explicitly,

$$ {}^4A^{-1} = \frac{a_6}{2\Delta}\,{}^4T_1 + \frac{1}{a_2}\,{}^4T_2 - \frac{a_3}{\Delta}\,{}^4T_3 - \frac{a_4}{\Delta}\,{}^4T_4 + \frac{4}{a_5}\,{}^4T_5 + \frac{2a_1}{\Delta}\,{}^4T_6,\ \ \Delta = 2\left(a_1a_6 - a_3a_4\right), \tag{23} $$

and double outer scalar products are given by

$$ \begin{aligned} {}^4A : {}^4B = \left(2a_1b_1 + a_3b_4\right){}^4T_1 + a_2b_2\,{}^4T_2 + \left(2a_1b_3 + a_3b_6\right){}^4T_3 + \\ + \left(2a_4b_1 + a_6b_4\right){}^4T_4 + \frac{1}{2}a_5b_5\,{}^4T_5 + \left(a_6b_6 + 2a_4b_3\right){}^4T_6\,. \end{aligned} \tag{24} $$

Unit tensors of fourth rank can also be spanned in this base:

$$ {}^41 = \frac{1}{2}\,{}^4T_1 + {}^4T_2 + 2\,{}^4T_5 + {}^4T_6,\ \ 11 = {}^4T_1 + {}^4T_3 + {}^4T_4 + {}^4T_6\,. \tag{25} $$

**Appendix (b):Hill’s and Property contribution tensors.** The homogenization is based on the solution for the Eshelby problem of an inhomogeneity. The region $V_1$, called the *inhomogeneity* (*i.e.*, the mesogens), has elastic properties $C_1$ or $S_1 = C_1^{-1}$ (the so-called *compliance tensor* fourth rank) that differ from those of the surrounding material, i.e., the polymer matrix ($C_0$ or $S_0 = C_0^{-1}$). In the present case we will assume both of them to be isotropic, The matrix is subjected to remotely applied loading by stress or strain, $\sigma_0$ or $\varepsilon_0$, respectively. The primary objective of this problem is to determine the resulting stresses and strains both inside and outside $V_1$, as well as the stress concentrations along its boundary. If $V_1$ is an ellipsoid, the solution can be expressed in a closed form using elliptic functions, which simplify to elementary functions when $V_1$ has the spheroidal shape. We are primarily interested in the strain and stress fields inside the inhomogeneity. For an ellipsoidal domain, the strain field is given by

$$ \varepsilon_{\text{in}} = {}^4\Lambda_\varepsilon : \varepsilon_0,\ \ {}^4\Lambda_\varepsilon = \left[{}^41 + {}^4P : \left(C_1 - C_0\right)\right]^{-1}, \tag{26} $$

where ${}^4\Lambda_{\text{in}}$ is the strain concentration tensor and ${}^4P$ is Hill's tensor which determines the strain at a point $x$:

$$ {}^4P = \left(\nabla \int_V G\left(x - x'\right)\nabla' dx'\right)^s_{(12)(34)}, \tag{27} $$

where s refers to the appropriate symmetrization and $G\left(x - x'\right)$ is the (known) Green’s function. For a spheroidal inhomogeneity ${}^4P$ remains constant within the interior points of $V_1$, which implies uniform strain within. Similarly,

$$ \sigma_{\text{in}} = {}^4\Lambda_\sigma : \sigma_0,\ \ {}^4\Lambda_\sigma = \left[{}^41 + {}^4Q : \left(S_1 - S_0\right)\right]^{-1}, \tag{28} $$

where the tensors ${}^4Q$ and ${}^4\Lambda_\sigma$ are defined as

$$ {}^4Q = C_0 - C_0 : {}^4P : C_0,\ \ {}^4\Lambda_\sigma = S_0 : {}^4\Lambda_\varepsilon : C_1\,. \tag{29} $$

Isotropic stiffnesses (for the polymer matrix and for the mesogens) are given by ($\lambda$ and $\mu$ are the two Lamé parameters):

$$ {}^4C = \lambda 11 + 2\mu\,{}^41 = \sum\nolimits_{i=1}^6 C_i\,{}^4T_i,\ \ C_1 = \lambda + \mu,\ \ C_2 = 2\mu,\ \ C_3 = C_4 = \lambda,\ \ C_5 = 4\mu,\ \ C_6 = \lambda + 2\mu\,. \tag{30} $$

For a spheroidal inhomogeneity the tensors ${}^4P$ and ${}^4Q$, are elementary functions of the aspect ratio $\gamma = a_3 / a$, namely,

$$ {}^4P = \sum\nolimits_{i=1}^6 p_i\left(\gamma\right){}^4T_i,\ \ {}^4Q = \sum\nolimits_{i=1}^6 q_i\left(\gamma\right){}^4T_1 \tag{31} $$

with

$$ \begin{aligned} p_1 = \frac{1}{2\mu}\left[\left(1-\kappa\right)f_0 + \kappa f_1\right],\ \ p_2 = \frac{1}{2\mu}\left[\left(2-\kappa\right)f_0 + \kappa f_1\right],\ \ p_3 = p_4 = -\frac{\kappa}{\mu}f_1, \\ p_5 = \frac{1}{\mu}\left[1 - f_0 - 4\kappa f_1\right],\ \ p_2 = \frac{1}{\mu}\left[\left(1-\kappa\right)\left(1-2f_0\right) + 2\kappa f_1\right],\ \ \kappa = \frac{\lambda+\mu}{\lambda+2\mu}, \end{aligned} \tag{32} $$

and

$$ \begin{aligned} q_1 = \mu\left[4\kappa - 2\left(3\kappa-1\right)f_0 - 2\kappa f_1\right],\ \ q_2 = 2\mu\left[1 - \left(2-\kappa\right)f_0 - \kappa f_1\right], \\ q_3 = q_4 = 2\mu\left[\left(2\kappa-1\right)f_0 + 2\kappa f_1\right],\ \ q_5 = 4\mu\left(f_0 + 4\kappa f_1\right),\ \ q_6 = 8\mu\kappa\left(f_0 - f_1\right), \end{aligned} \tag{33} $$

where for a prolate inclusion (as in the case of the mesogens) we must put

$$f_0 = \frac{\gamma^2}{2\left(\gamma^2-1\right)}\left(1-\frac{1}{2\gamma\sqrt{\gamma^2-1}}\ln\frac{\gamma+\sqrt{\gamma^2-1}}{\gamma-\sqrt{\gamma^2-1}}\right),\ f_1 = \frac{\gamma^2}{4\left(\gamma^2-1\right)^2}\left[\left(2\gamma^2+1\right)\frac{1}{2\gamma\sqrt{\gamma^2-1}}\ln\frac{\gamma+\sqrt{\gamma^2-1}}{\gamma-\sqrt{\gamma^2-1}}-3\right]. \tag{34}$$

The next important concept is the property contribution tensors, which describe the contribution of an inhomogeneity to the effective property of interest. This is done under the assumption that the inhomogeneity is embedded in a uniform applied, $\sigma_0$ or $\varepsilon_0$ (tractions or displacements on the RVE have the form $t\big|_{\partial V} = n\cdot\sigma_0$ or $u\big|_{\partial V} = x\cdot\varepsilon_0$). We consider an RVE, $V$, containing an isolated inhomogeneity of volume $V_1$ (the mesogen) The volume-averaged stress and strain fields can be expressed as

$$\langle\sigma\rangle = C_0 : \varepsilon_0 + \Delta\sigma,\ \langle\varepsilon\rangle = S_0 : \sigma_0 + \Delta\varepsilon\,. \tag{35}$$

Since the material is assumed to be linearly elastic, the additional stress and strain contributions due to the inhomogeneity are linear functions of the applied field:

$$\Delta\sigma = {}^4N : \varepsilon_0,\ \Delta\varepsilon = {}^4H : \sigma_0, \tag{36}$$

where ${}^4N$ and ${}^4H$ are the so-called stiffness and compliance contribution tensors.

For an ellipsoidal inhomogeneity, the property contribution tensors can be expressed in terms of Hill's tensors, which provide the average field inside the inhomogeneity in terms of the applied field. By introducing the strain averages over the inhomogeneity, $\langle\varepsilon\rangle_{\text{in}}$, and over the matrix, $\langle\varepsilon\rangle_{\text{out}}$, we obtain

$$\langle\varepsilon\rangle = \frac{V-V_1}{V}\langle\varepsilon\rangle_{\text{out}} + \frac{V_1}{V}\langle\varepsilon\rangle_{\text{in}} = \frac{V-V_1}{V}S_0 : \langle\sigma\rangle_{\text{out}} + \frac{V_1}{V}S_1 : \langle\sigma\rangle_{\text{in}}\,. \tag{37}$$

By expressing $\langle\sigma\rangle_{\text{out}}$ from the relation

$$\frac{V_1}{V}\langle\sigma\rangle_{\text{in}} + \frac{V-V_1}{V}\langle\sigma\rangle_{\text{out}} = \sigma_0 \tag{38}$$

we obtain

$$\langle\varepsilon\rangle = S_0 : \sigma_0 + \frac{V_1}{V}\left(S_1 - S_0\right) : \langle\sigma\rangle_{\text{in}} = S_0 : \sigma_0 + \langle\sigma\rangle_{\text{out}} + \frac{V_1}{V}\left(S_1 - S_0\right) : {}^4\Lambda_\sigma : \sigma_0 \tag{39}$$

so that

$$ {}^4H = \frac{V_1}{V}\left(S_1 - S_0\right) : {}^4\Lambda_\sigma\,. \tag{40}$$

Using $(28)_2$ we conclude that

$$ {}^4\Lambda_\sigma = \left[{}^41 + {}^4Q : \left(S_1 - S_0\right)\right]^{-1} \Rightarrow {}^4H = \frac{V_1}{V}\left[\left(S_1 - S_0\right)^{-1} + {}^4Q\right]^{-1}. \tag{41}$$

A similar procedure applies for stresses, leading to the stiffness contribution tensor,

$$ {}^4N = \frac{V_1}{V}\left(C_1 - C_0\right) : {}^4\Lambda_\varepsilon\,, \tag{42}$$

and with $(26)_2$:

$$ {}^4\Lambda_\varepsilon = \left[{}^41 + {}^4P : \left(C_1 - C_0\right)\right]^{-1} \Rightarrow {}^4N = \frac{V_1}{V}\left[\left(C_1 - C_0\right)^{-1} + {}^4P\right]^{-1}. \tag{43}$$

So far only one inclusion was involved. Now let us assume there are many inclusion types labeled by the index $k$. The simplest approximation is to assume *no interaction*, such that the inhomogeneities are treated as isolated entities, and interactions between neighbors are neglected. In this approximation, the property contribution tensors weighted by volume fractions simply sum up, and (36) reads:

$$\Delta C = \left(\Sigma_k\ {}^4N_k\right),\ \Delta S = \left(\Sigma_k\ {}^4H_k\right)\ \text{in}\ \Delta\sigma = \Delta C : \varepsilon_0,\ \Delta\varepsilon = \Delta S : \sigma_0\,. \tag{44}$$

In comparison with (35) we obtain the homogenized stiffness

$$C_{\text{hom}} = C_0 + \left(\Sigma_k\ {}^4N_k\right),\ S_{\text{hom}} = S_0 + \left(\Sigma_k\ {}^4H_k\right). \tag{45}$$

In this equation we still allow that each type of inclusion has different contribution tensors,

$$ {}^4N_k = \frac{V_k}{V}\left[\left(C_k - C_0\right)^{-1} + {}^4P_k\right]^{-1},\ {}^4H_k = \frac{V_k}{V}\left[\left(S_k - S_0\right)^{-1} + {}^4Q_k\right]^{-1}. \tag{46}$$

It should be noted that the inclusion types can have different aspect ratios and be oriented differently, ${}^4P_k = {}^4P_k\left(\gamma_k, m_k\right)$, ${}^4Q_k = {}^4Q_k\left(\gamma_k, m_k\right)$. In order to prepare for continuous distributions, we now assume that all types of inclusions contribute with the same volume fraction $\Delta V$, so that $p = \frac{1}{V}\Sigma_k\, V_k = \frac{k\Delta V}{V}$ represents the total volume fraction of inclusions. Let us further replace the summation of the property contribution tensors by integration over orientations using the distribution function from Eq. (1). Similarly, as in Eq. (5), we then obtain

$$\left\langle {}^4\overline{N} \right\rangle = \int_\Phi {}^4\overline{N} \psi_\lambda (\varphi, \theta) d\Phi, \quad {}^4\overline{N} = \left[ \left( C_1 - C_0 \right)^{-1} + {}^4P \right]^{-1}, \quad C_{\text{hom}} = C_0 + p \left\langle {}^4\overline{N} \right\rangle, \tag{47}$$

and

$$\left\langle {}^4\overline{N} \right\rangle = \int_\Phi {}^4\overline{N} \psi_\lambda (\varphi, \theta) d\Phi, \quad {}^4\overline{H} = \left[ \left( S_1 - S_0 \right)^{-1} + {}^4Q \right]^{-1}, \quad S_{\text{hom}} = S_0 + p \left\langle {}^4\overline{H} \right\rangle. \tag{48}$$

This is the *Non-Interaction-Approximation* (NIA) for the case of a continuous randomized distribution of inclusions all of the same stiffness and compliance, $C_1$, $S_1$, respectively. It holds for $p$-values that are not too large, say 1 % – 10 %. Note that the property contribution tensors $\left\langle {}^4\overline{N} \right\rangle$ and $\left\langle {}^4\overline{H} \right\rangle$ are transversely isotropic tensors of the fourth rank depending on the orientation parameter $\lambda$.

The NIA homogenization can be improved: in the advanced *Mori-Tanaka schemes* (see [18], Section 5.6.2) the interactions between inhomogeneities are accounted for by placing the inhomogeneities–treated as isolated ones–into a uniform field that is equal to its average over the matrix part of the composite and that generally differs from the remotely applied one. Then the effective elastic stiffness and compliances are given by:

$$C_{\text{hom}} = C_0 + p \left( p \left( C_1 - C_0 \right)^{-1} + (1-p) \left\langle {}^4\overline{N} \right\rangle^{-1} \right)^{-1}, \quad S_{\text{hom}} = S_0 + p \left( p \left( S_1 - S_0 \right)^{-1} + (1-p) \left\langle {}^4\overline{H} \right\rangle^{-1} \right)^{-1}. \tag{49}$$

If the inclusions are rigid (as the mesogens are when compared to the matrix) these equations simplify:

$$C_{\text{hom}} = C_0 + \frac{p}{1-p} \left\langle {}^4\overline{P} \right\rangle, \quad S_{\text{hom}} = S_0 + \frac{p}{1-p} \left\langle {}^4\overline{Q} \right\rangle^{-1}. \tag{50}$$

**Appendix (c): Mori-Tanaka scheme for thermal expansion.** For homogenization of the thermal expansion coefficients $\alpha$ similar ideas as in the previous Appendix apply: each inhomogeneity is treated as an isolated one placed into a uniform stress field that is equal to its average over the matrix part of the heterogeneous material, $\sigma_* = \langle \sigma \rangle_m$, and that generally differs from the remote stress $\sigma_0$. The stress averaged over the RVE reads:

$$\sigma_0 = \langle \sigma \rangle = \Sigma_k \left[ p_k \langle \sigma \rangle_k + (1 - p_k) \langle \sigma \rangle_m \right], \quad p_k = \frac{V_k}{V}. \tag{51}$$

According to the basic idea of Mori-Tanaka scheme stresses within an inhomogeneity is defined as

$$\sigma(x) = \sigma_* - \int_{V_k} {}^4Z(x - x') : \left[ (S_k - S_0) : \sigma(x') + (\alpha_k - \alpha_0) \langle \sigma \rangle_m \right], \quad p_k = \frac{V_k}{V},$$

$${}^4Z(x - x') = C_0 : \left[ \nabla G(x - x') \nabla' \right] : C_0 - C_0 \delta(x'). \tag{52}$$

Note that later we will assume that the tensors of thermal expansion of the inclusions and of the matrix (i.e., $\alpha_k$ and $\alpha_0$, respectively) are isotropic. $\Delta T$ denotes the temperature change. If the domains $V_k$ are ellipsoidal then the stresses inside are uniform and therefore

$$\sigma(x) = \sigma_* - {}^4Q_k : \left[ (S_k - S_0) : \langle \sigma \rangle_k + (\alpha_k - \alpha_0) \Delta T \right],$$

$${}^4Q_k(\gamma_k, m_k) = C_0 - C_0 : {}^4P_k(\gamma_k, m_k) : C_0, \quad {}^4P_k(\gamma_k, m_k) = \left( \nabla \int_{V_k} G(x - x') \nabla' dx' \right)^3_{(12)(34)}. \tag{53}$$

It follows that

$$\langle \sigma \rangle_k = {}^4\Lambda_k^\sigma : \left[ \sigma_* - {}^4Q_k : (\alpha_k - \alpha_0) \Delta T \right], \quad {}^4\Lambda_k^\sigma = \left[ {}^41 + {}^4Q_k : (S_k - S_0) \right]^{-1}, \tag{54}$$

and therefore from (51):

$$\sigma_0 = \Sigma_k \left[ p_k \, {}^4\Lambda_k^\sigma + (1 - p_k) \, {}^41 \right] : \sigma_* - \Sigma_k \left[ p_k \, {}^4\Lambda_k^\sigma : {}^4Q_k : (\alpha_k - \alpha_0) \Delta T \right] \tag{55}$$

or

$$\sigma_* = \left[ \Sigma_k \left( p_k \, {}^4\Lambda_k^\sigma + (1 - p_k) \, {}^41 \right) \right]^{-1} : \left\{ \sigma_0 + \Sigma_k \left[ p_k \, {}^4\Lambda_k^\sigma : {}^4Q_k : (\alpha_k - \alpha_0) \Delta T \right] \right\} \tag{56}$$

and so

$$\langle \sigma \rangle_i = {}^4\Lambda_i^\sigma : \left\{ \left[ \Sigma_k \left( p_k \, {}^4\Lambda_k^\sigma + (1 - p_k) \, {}^41 \right) \right]^{-1} : \left( \sigma_0 + \Sigma_k \left[ p_k \, {}^4\Lambda_k^\sigma : {}^4Q_k : (\alpha_k - \alpha_0) \Delta T \right] \right) - {}^4Q_i : (\alpha_i - \alpha_0) \Delta T \right\} \tag{57}$$

The strain averaged over the RVE is given by

$$\langle \varepsilon \rangle = \Sigma_k \left[ p_k \langle \varepsilon \rangle_k + (1 - p_k) \langle \varepsilon \rangle_m \right] = \Sigma_k \left[ p_k \left( S_k : \langle \sigma \rangle_k + \alpha_k \Delta T \right) + (1 - p_k) \left( S_0 : \langle \sigma \rangle_m + \alpha_0 \Delta T \right) \right]. \tag{58}$$

We now take into account that

$$\left(1-p_k\right)\langle\sigma\rangle_m=\sigma_0-\Sigma_k p_k\langle\sigma\rangle_k . \tag{59}$$

and find with (55):

$$\begin{aligned}\langle\varepsilon\rangle&=S_0:\sigma_0+\alpha_0\Delta T+\Sigma_k p_k\left[\left(S_k-S_0\right)^{-1}:\langle\sigma\rangle_k+\left(\alpha_k-\alpha_0\right)\Delta T\right]=\\&=S_0:\sigma_0+\alpha_0\Delta T+\left\{\Sigma_k p_k\,{}^4H_k:\left[p_k\left(S_k-S_0\right)^{-1}:{}^4H_k+\left(1-p_k\right){}^41\right]^{-1}\right\}:\sigma_0+\\&=\Sigma_k\left(p_k\,{}^4H_k:\left\{\Sigma_k\left[p_k\left(S_k-S_0\right)^{-1}:{}^4H_k+\left(1-p_k\right){}^41\right]\right\}^{-1}\right):\Sigma_k\left[p_k\,{}^4\Lambda_k^\sigma:{}^4Q_k:\left(\alpha_k-\alpha_0\right)\Delta T\right]+\\&\quad+\Sigma_k\left[p_k\left({}^41-{}^4H_k:{}^4Q_k\right):\left(\alpha_k-\alpha_0\right)\Delta T\right].\end{aligned} \tag{60}$$

We note that

$${}^4H_k=\left(S_k-S_0\right):{}^4\Lambda_k^\sigma=\left[\left(S_k-S_0\right)^{-1}+{}^4Q_k\right]^{-1}. \tag{61}$$

We define

$${}^41-{}^4H_k:{}^4Q_k={}^4H_k:\left({}^4H_k^{-1}-{}^4Q_k\right)={}^4H_k:\left(S_k-S_0\right)^{-1}={}^4\overline{H}_{Tk} \tag{62}$$

and conclude

$${}^4\Lambda_k^\sigma:{}^4Q_k=\left(S_k-S_0\right)^{-1}:{}^4H_k:{}^4Q_k=\left(S_k-S_0\right)^{-1}:\left({}^41-{}^4\overline{H}_{Tk}\right). \tag{63}$$

Let us finally consider a two-phase material with identical inhomogeneities and assume that the inhomogeneities distribution over size is statistically independent of the distribution over orientation. Then after recalling (48) and adjust ${}^4\overline{H}_k\to{}^4\overline{H}_{Tk}$ or rather $\left\langle{}^4\overline{H}\right\rangle\to\left\langle{}^4\overline{H}_T\right\rangle$ we get:

$$\Sigma_k\left(p_k\,{}^4H_k\right):\left\{\Sigma_k\left[p_k\left(S_k-S_0\right)^{-1}:{}^4H_k+\left(1-p_k\right){}^41\right]\right\}^{-1}=p\left[p\left(S_1-S_0\right)^{-1}+\left(1-p\right)\left\langle{}^4\overline{H}\right\rangle^{-1}\right]^{-1} \tag{64}$$

recover $(49)_2$ and obtain finally

$$\alpha_{\text{hom}}=\alpha_0+p\left\{\left[p\,{}^41+\left(1-p\right)\left\langle{}^4\overline{H}_T\right\rangle^{-1}\right]^{-1}:\left({}^41-\left\langle{}^4\overline{H}_T\right\rangle^{-1}\right)+\left\langle{}^4\overline{H}_T\right\rangle^{-1}\right\}:\left(\alpha_1-\alpha_0\right)\Delta T . \tag{65}$$

It should be noted that the Mori-Tanaka scheme for thermal expansion seems to be less known than the one for stiffnesses, since articles on it have been published relatively recently, [33].

**Acknowledgments.** This work was financially supported bd DFG (Deutsche Forschungsgemeinschaft) under project MU 1752/68-1 525235558 for LS and ENV, which is most gratefully acknowledged.

## Bibliography

1. *Mahmood A.*, *Perveen F.*, *Chen S.*, *Akram T.*, *Irfan A.* Polymer Composites in 3D/4D Printing: Materials, Advances, and Prospects // Molecules. – 2024. – Vol. 29. – no. 2. – P. 319. DOI: 10.3390/molecules29020319.
2. *Wang Y.*, *Yang H.*, *Qi H. J.*, *Fang D.* Recent advances in molecular programming of liquid crystal elastomers with additive manufacturing for 4D printing // Mol. Syst. Des. Eng. – 2022. – Vol. 7. – no. 5. – P. 511 – 533. DOI: 10.1039/D2ME00124A.
3. *Bae J.*, *Kang S. H.*, *Ryu M.*, *Kim Y.*, *Kim Y. T.* Advances in 4D printing of liquid crystalline elastomers: materials, techniques, and applications // Mater. Horiz. – 2022. – Vol. 9. – no. 10. – P. 2756 – 2774. DOI: 10.1039/D2MH00232A.
4. *Liao Y.*, *Wang Y.*, *Wang Z.*, *Li Y.*, *Yang H.* 4D Printing of Shape-Morphing Liquid Crystal Elastomers // Chem. Bio. Eng. – 2024. – Vol. 11. – no1. – P. 1 – 15. DOI: 10.1021/cbe.4c00027.
5. *Wang J.*, *Li C.*, *Yuan C.*, *Li Y.*, *Wang Z.*, *Yang H.* 4D printing of a liquid crystal elastomer with a controllable orientation gradient // ACS Appl. Mater. Interfaces. – 2020. – Vol. 12. – no. 18. – P. 20819 – 20827. DOI: 10.1021/acsami.9b18037.
6. *Gelebart A. H.*, *Vantomme G.*, *Meijer E. W.*, *Broer D. J.* Mastering the photothermal effect in liquid crystal networks: A general approach for self-sustained mechanical oscillators // Adv. Mater. – 2017. – Vol. 29. – no. 43. – P. 1606712. DOI: 10.1002/adma.201606712.
7. *Zeng H.*, *Wasylczyk P.*, *Wiersma D. S.*, *Priimagi A.* Light robots: Bridging the gap between microrobotics and photomechanics in soft materials // Adv. Mater. – 2018. – Vol. 30. – no. 44. – P. 1703554. DOI: 10.1002/adma.201703554.
8. *Zhu W.*, *Shelley M.*, *Palffy-Muhoray P.* Modeling and simulation of liquid-crystal elastomers // Phys. Rev. E. – 2011. – Vol. 83. – no. 5. – P. 051703. DOI: 10.1103/PhysRevE.83.051703.
9. *Goriely A.*, *Taffetani M.* A pseudo-anelastic model for stress softening in liquid crystal elastomers // Proc. R. Soc. A. – 2021. – Vol. 477. – no. 2250. – P. 20200558.
10. *Taffetani M.*, *Goriely A.* A mathematical model for the auxetic response of liquid crystal elastomers // Philos. Trans. R. Soc. A. – 2022. – Vol. 380. – no. 2218. – P. 20210326. DOI: 10.1098/rsta.2021.0326.
11. *Lee K.*, *Kim J.* Numerical simulation and experimental validation of bending and curling behaviors of liquid crystal elastomer beams under thermal actuation // Appl. Phys. Lett. – 2021. – Vol. 118. – no. 24. – P. 241903. DOI: 10.1063/5.0054243.
12. *Zhang J.*, *Wang Y.*, *Li Y.*, *Yang H.* Morphing of stiffness-heterogeneous liquid crystal elastomers via mechanical training and locally controlled photopolymerization // Matter. – 2022. – Vol. 5. – no. 9. – P. 3133 – 3147. DOI: 10.1016/j.matt.2022.07.002.

13. *Skačeja M.*, *Zannoni C.* Molecular simulations elucidate electric field actuation in swollen liquid crystal elastomers // Proc. Natl. Acad. Sci. U.S.A. – 2012. – Vol. 109. – no. 14. – P. 5134 – 5139. DOI: 10.1073/pnas.1121235109.
14. *Yamamoto T.*, *Takahashi M.*, *Yamaguchi T.* Regression analysis for predicting the elasticity of liquid crystal elastomers // Polymers. – 2022. – Vol. 14. – no. 23. – P. 5192. DOI: 10.3390/polym14235192.
15. *Oates W. S.*, *Smith R. C.* Phase field modeling of domain evolution in liquid crystal elastomers // Polymers. – 2021. – Vol. 13. – no. 10. – P. 1650. DOI: 10.3390/polym13101650.
16. *Bartels S.*, *Griehl M.*, *Keck J.*, *Neukamm S.* Modeling and simulation of nematic LCE rods // arXiv preprint. – 2022. – arXiv:2205.15174. – Режим доступу : https://arxiv.org/abs/2205.15174. – Дата звертання : 25 травня 2025 р.
17. *Eringen A. C.* Microcontinuum Field Theories I: Foundations and Solids. – New York : Springer-Verlag, 1999. – 325 p.
18. *Kachanov M.*, *Sevostianov I.* Micromechanics of materials, with applications. 0925-0042; 249. – Springer, 2018. – 712 p.
19. *Moran B. D.*, *Lee E.*, *Krikorian C. C.*, *Bekker L.* Patent US11794406B1, United States. Stereolithography Additive Manufacturing of Photoaligned Liquid Crystal Elastomers. patents.google.com. – Lawrence Livermore National Security LLC, 2023.
20. *Stupkiewicz S.*, *Maciejewski G.*, *Petryk H.* Elastic micro-strain energy of austenite–martensite interface in NiTi // Modelling and Simulation in Materials Science and Engineering. – 2012. – Vol. 20. – no. 3. – P. 035001. DOI: 10.1088/0965-0393/20/3/035001.
21. *Johnston I. D.*, *McCluskey D. K.*, *Tan C. K. L.*, *Tracey M. C.* Mechanical characterization of bulk Sylgard 184 for microfluidics and microengineering // Journal of Micromechanics and Microengineering. – 2014. – Vol. 24. – No. 3. – P. 035017. DOI: 10.1088/0960-1317/24/3/035017.
22. *Ganicz T.*, *Stańczyk W.* Side-chain liquid crystal polymers (SCLCP): Methods and materials. An overview // Materials. – 2009. – Vol. 2. – no. 1. – P. 95 – 128. DOI: 10.3390/ma2010095.
23. *Farren C.*, *Akatsuka M.*, *Takezawa Y.*, *Itoh Y.* Thermal and mechanical properties of liquid crystalline epoxy resins as a function of mesogen concentration // Polymer. – 2001. – Vol. 42. – no. 4. – P. 1507 – 1514. DOI: 10.1016/S0032-3861(00)00481-2.
24. *Sgotti V. J.*, *Reis C. M.*, *Molter R.*, *Vinciguerra M.*, *Yao L.*, *Majidi C.*, *Tavakoli M.* Toward Fully Printed Soft Actuators: UV-Assisted Printing of Liquid Crystal Elastomers and Biphasic Liquid Metal Conductors // Advanced Materials Technologies. – 2023. – Vol. 8. – No. 15. – P. 2300144. DOI: 10.1002/admt.202300144.
25. *Zang T.*, *Fu S.*, *Cheng J.*, *Zhang C.*, *Lu X.*, *Hu J.*, *Xia H.*, *Zhao Y.* 4D printing of shape-morphing liquid crystal elastomers // Chem & Bio Engineering. – 2024. – Vol. 1. – No. 6. – P. 488 – 515. DOI: https://doi.org/10.1021/cbe500018e.
26. *Da Cunha M. P.*, *Debije M. G.*, *Schenning A. P. H. J.* Bioinspired light-driven soft robots based on liquid crystal polymers // Chemical Society Reviews. – 2020. – Vol. 49. – no. 18. – P. 6568 – 6578. DOI: https://doi.org/10.1039/D0CS00435A.
27. *Roach D. J.*, *Kuang X.*, *Yuan C.*, *Chen K.*, *Qi H. J.* Novel ink for ambient condition printing of liquid crystal elastomers for 4D printing // Smart Materials and Structures. – 2018. – Vol. 27. – no. 12. – P. 125011. DOI: 10.1088/1361-665X/aae9fa.
28. *Ryan K. R.*, *Down M. P.*, *Banks C. E.* Future of additive manufacturing: Overview of 4D and 3D printed smart and advanced materials and their applications // Chemical Engineering Journal. – 2021. – Vol. 403. – P. 126162. DOI: 10.1016/j.cej.2020.126162.
29. *Momeni F.*, *Liu X.*, *Ni J.* A review of 4D printing // Materials & Design. – 2017. – Vol. 122. – P. 42 – 79. DOI: 10.1016/j.matdes.2017.02.068.
30. *Logg A.*, *Mardal K.-A.*, *Wells G. N.* Automated Solution of Differential Equations by the Finite Element Method: The FEniCS Book. – Springer, 2012. – 731 p.
31. *Qiu W.*, *He X.*, *Fang Z.*, *Wang Y.*, *Dong K.*, *Zhang G.*, *Xu X.*, *Ge Q.*, *Xiong Y.* Shape-tunable 4D printing of LCEs via cooling rate modulation: stimulus-free locking of actuated state at room temperature // ACS Applied Materials & Interfaces. – 2023. – Vol. 15. – № 40. – P. 47509 – 47519. DOI: 10.1021/acsami.3c14589.
32. *Kang W.*, *Cheng Q.*, *Liu C.*, *Wang Z.*, *Li D.*, *Liang X.* A constitutive model of monodomain liquid crystal elastomers with the thermal-mechanical-nematic order coupling // Journal of the Mechanics and Physics of Solids. – 2025. – Vol. 196. – P. 105995. DOI: 10.1016/j.jmpc.2024.105995.
33. *Lu P.* Further studies on Mori–Tanaka models for thermal expansion coefficients of composites // Polymer. – 2013. – Vol. 54. – no. 6. – P. 1691 – 1699. DOI: 10.1016/j.polymer.2013.01.057.

**References (transliterated)**

1. Mahmood A., Perveen F., Chen S., Akram T., Irfan A. Polimerni kompozyty v 3D/4D-druku: materially, dosyagnennya ta perspektyvy [Polymer Composites in 3D/4D Printing: Materials, Advances, and Prospects]. *Molecules*. 2024, Vol. 29, no. 2, P. 319. DOI: 10.3390/molecules29020319.
2. Wang Y., Yang H., Qi H. J., Fang D. Recent advances in molecular programming of liquid crystal elastomers with additive manufacturing for 4D printing. *Mol. Syst. Des. Eng*. 2022, Vol. 7, no. 5, pp. 511–533. DOI: 10.1039/D2ME00124A.
3. Bae J., Kang S. H., Ryu M., Kim Y., Kim Y. T. Advances in 4D printing of liquid crystalline elastomers: materials, techniques, and applications. *Mater. Horiz*. 2022, Vol. 9, no. 10, pp. 2756–2774. DOI: 10.1039/D2MH00232A.
4. Liao Y., Wang Y., Wang Z., Li Y., Yang H. 4D Printing of Shape-Morphing Liquid Crystal Elastomers. *Chem. Bio. Eng*. 2024, Vol. 11, no. 1, pp. 1–15. DOI: 10.1021/cbe.4c00027.
5. Wang J., Li C., Yuan C., Li Y., Wang Z., Yang H. 4D printing of a liquid crystal elastomer with a controllable orientation gradient. *ACS Appl. Mater. Interfaces*. 2020, Vol. 12, no. 18, pp. 20819–20827. DOI: 10.1021/acsami.9b18037.
6. Gelebart A. H., Vantomme G., Meijer E. W., Broer D. J. Mastering the photothermal effect in liquid crystal networks: A general approach for self-sustained mechanical oscillators. *Adv. Mater*. 2017, Vol. 29, no. 43, P. 1606712. DOI: 10.1002/adma.201606712.
7. Zeng H., Wasylczyk P., Wiersma D. S., Priimagi A. Light robots: Bridging the gap between microrobotics and photomechanics in soft materials. *Adv. Mater*. 2018, Vol. 30, no. 44. P. 1703554. DOI: 10.1002/adma.201703554.
8. Zhu W., Shelley M., Palffy-Muhoray P. Modeling and simulation of liquid-crystal elastomers. *Phys. Rev. E*. 2011, Vol. 83, no. 5, P. 051703. DOI: 10.1103/PhysRevE.83.051703.
9. Goriely A., Taffetani M. A pseudo-anelastic model for stress softening in liquid crystal elastomers. *Proc. R. Soc. A*. 2021, Vol. 477, no. 2250, P. 20200558.
10. Taffetani M., Goriely A. A mathematical model for the auxetic response of liquid crystal elastomers. *Philos. Trans. R. Soc. A*. 2022, Vol. 380, no. 2218, P. 20210326. DOI: 10.1098/rsta.2021.0326.
11. Lee K., Kim J. Numerical simulation and experimental validation of bending and curling behaviors of liquid crystal elastomer beams under thermal actuation. *Appl. Phys. Lett*. 2021, Vol. 118, no. 24, P. 241903. DOI: 10.1063/5.0054243.
12. Zhang J., Wang Y., Li Y., Yang H. Morphing of stiffness-heterogeneous liquid crystal elastomers via mechanical training and locally controlled photopolymerization. *Matter*. 2022, Vol. 5, no. 9, pp. 3133–3147. DOI: 10.1016/j.matt.2022.07.002.
13. Skačeja M., Zannoni C. Molecular simulations elucidate electric field actuation in swollen liquid crystal elastomers. *Proc. Natl. Acad. Sci. U.S.A*. 2012, Vol. 109, no. 14, pp. 5134–5139. DOI: 10.1073/pnas.1121235109.
14. Yamamoto T., Takahashi M., Yamaguchi T. Regression analysis for predicting the elasticity of liquid crystal elastomers. *Polymers*. 2022, Vol. 14, no. 23, P. 5192. DOI: 10.3390/polym14235192.
15. Oates W. S., Smith R. C. Phase field modeling of domain evolution in liquid crystal elastomers. *Polymers*. 2021, Vol. 13, no. 10, P. 1650. DOI: 10.3390/polym13101650.
16. Bartels S., Griehl M., Keck J., Neukamm S. *Modeling and simulation of nematic LCE rods*. arXiv preprint. 2022. arXiv:2205.15174. Available at: https://arxiv.org/abs/2205.15174. (accessed 25 May 2025).

**17.** Eringen A. C. *Microcontinuum Field Theories I: Foundations and Solids*. New York, Springer-Verlag, 1999. 325 p

**18.** Kachanov M., Sevostianov I. *Micromechanics of materials, with applications.* 0925-0042; 249. Springer, 2018. 712 p.

**19.** Moran B. D., Lee E., Krikorian C. C., Bekker L. Stereolithography Additive Manufacturing of Photoaligned Liquid Crystal Elastomers. patents.google.com. Patent United States, Lawrence Livermore National Security LLC, no. US11794406B1, 2023.

**20.** Stupkiewicz S., Maciejewski G., Petryk H. Elastic micro-strain energy of austenite–martensite interface in NiTi. *Modelling and Simulation in Materials Science and Engineering*. 2012, Vol. 20, no. 3, P. 035001. DOI: 10.1088/0965-0393/20/3/035001.

**21.** Johnston I. D., McCluskey D. K., Tan C. K. L., Tracey M. C. Mechanical characterization of bulk Sylgard 184 for microfluidics and microengineering. *Journal of Micromechanics and Microengineering*. 2014, Vol. 24, No. 3, P. 035017. DOI: 10.1088/0960-1317/24/3/035017.

**22.** Ganicz T., Stańczyk W. Side-chain liquid crystal polymers (SCLCP): Methods and materials. An overview. *Materials*. 2009, Vol. 2, no. 1, pp. 95–128. DOI: 10.3390/ma2010095.

**23.** Farren C., Akatsuka M., Takezawa Y., Itoh Y. Thermal and mechanical properties of liquid crystalline epoxy resins as a function of mesogen concentration. *Polymer*. 2001, Vol. 42, no. 4, pp. 1507–1514. DOI: 10.1016/S0032-3861(00)00481-2.

**24.** Sgotti V. J., Reis C. M., Molter R., Vinciguerra M., Yao L., Majidi C., Tavakoli M. Toward Fully Printed Soft Actuators: UV-Assisted Printing of Liquid Crystal Elastomers and Biphasic Liquid Metal Conductors. *Advanced Materials Technologies*. 2023, Vol. 8, No. 15, P. 2300144. DOI: 10.1002/admt.202300144.

**25.** Zang T., Fu S., Cheng J., Zhang C., Lu X., Hu J., Xia H., Zhao Y. 4D printing of shape-morphing liquid crystal elastomers. *Chem & Bio Engineering*. 2024, Vol. 1, No. 6, pp. 488–515. DOI: https://doi.org/10.1021/cbe500018e.

**26.** Da Cunha M. P., Debije M. G., Schenning A. P. H. J. Bioinspired light-driven soft robots based on liquid crystal polymers // Chemical Society Reviews. – 2020. – Vol. 49. – no. 18. – P. 6568 – 6578. DOI: https://doi.org/10.1039/D0CS00435A.

**27.** Roach D. J., Kuang X., Yuan C., Chen K., Qi H. J. Novel ink for ambient condition printing of liquid crystal elastomers for 4D printing. *Smart Materials and Structures*. 2018, Vol. 27, no. 12, P. 125011. DOI: 10.1088/1361-665X/aae9fa.

**28.** Ryan K. R., Down M. P., Banks C. E. Future of additive manufacturing: Overview of 4D and 3D printed smart and advanced materials and their applications. *Chemical Engineering Journal*. 2021, Vol. 403, P. 126162. DOI: 10.1016/j.cej.2020.126162.

**29.** Momeni F., Liu X., Ni J. A review of 4D printing. *Materials & Design*. 2017, Vol. 122, P. 42–79. DOI: 10.1016/j.matdes.2017.02.068.

**30.** Logg A., Mardal K.-A., Wells G. N. Automated Solution of Differential Equations by the Finite Element Method: The FEniCS Book. Springer, 2012. 731 p.

**31.** Qiu W., He X., Fang Z., Wang Y., Dong K., Zhang G., Xu X., Ge Q., Xiong Y. Shape-tunable 4D printing of LCEs via cooling rate modulation: stimulus-free locking of actuated state at room temperature. *ACS Applied Materials & Interfaces*. 2023, Vol. 15, no. 40, pp. 47509–47519. DOI: 10.1021/acsami.3c14589.

**32.** Kang W., Cheng Q., Liu C., Wang Z., Li D., Liang X. A constitutive model of monodomain liquid crystal elastomers with the thermal-mechanical-nematic order coupling. *Journal of the Mechanics and Physics of Solids*. 2025, Vol. 196, P. 105995. DOI: 10.1016/j.jmpc.2024.105995.

**33.** Lu P. Further studies on Mori–Tanaka models for thermal expansion coefficients of composites. *Polymer*. 2013, Vol. 54, no. 6, pp. 1691–1699. DOI: 10.1016/j.polymer.2013.01.057.

*Надійшла (received) 30.05.2025*

## Відомості про авторів / Information about authors

***Шек Лука*** – аспірант, Технічний університет Берліна, Інститут механіки, LKM, Einsteinufer 5, 10587 Берлін; тел.: + 49 (30) 314-778-06; ORCID: https://orcid.org/0009-0002-2544-3185; e-mail: l.schek@ tu-berlin.de.

***Lucca Schek*** – Ph.D. candidate, Technische Universität Berlin, Institut für Mechanik, LKM, Einsteinufer 5, 10587 Berlin; tel.: + 49 (30) 314-778-06; ORCID: https://orcid.org/0009-0002-2544-3185; e-mail: l.schek@tu-berlin.de.

***Вільчевська Олена Микитівна –*** гостьовий професор та стипендіат програми Меркатор, Технічний університет Берліна, Інститут механіки, LKM, Einsteinufer 5, 10587 Берлін; тел.: + 49 (30) 314-276-82; ORCID: https://orcid.org/0000-0002-5173-3218; e-mail: vilchevska@gmail.com.

***Vilchevskaya Elena Nikitichna*** – Guest Professor and Mercator Follow, Technische Universität Berlin, Institut für Mechanik, LKM, Einsteinufer 5, 10587 Berlin; tel.: + 49 (30) 314-276-82; ORCID: https://orcid.org/0000-0002-5173-3218; e-mail: vilchevska@gmail.com.

***Мюллер Вольфганг Гельмут*** – професор та завідувач кафедри механіки суцільних середовищ та теорії конститутивних рівнянь, Технічний університет Берліна, Інститут механіки, LKM, Einsteinufer 5, 10587 Берлін; тел.: + 49 (30) 314-276-82; ORCID: https://orcid.org/0000-0003-0880-0726; e-mail: wolfgang.h.mueller@ tu-berlin.de.

***Wolfgang Helmut Müller*** – Professor and Chair of Continuum Mechanics and Constitutive Theory, Technische Universität Berlin, Institut für Mechanik, LKM, Einsteinufer 5, 10587 Berlin; tel.: + 49 (30) 314-276-82; ORCID: https://orcid.org/0000-0003-0880-0726; e-mail: wolfgang.h.mueller@tu-berlin.de.